Design of an Acoustic Shielding Flap Concept with Prediction and Validation

Ian A. Clark[1], Yueping Guo[2], and Russell H. Thomas[2]
NASA Langley Research Center, Hampton, VA 23681, USA

As part of a NATO task group, NASA has designed a noise reduction technology called a Shielding Flap for application to a hybrid wing body aircraft concept. The design drivers and objectives for this technology are outlined in this paper. Design parameters are defined, and recently developed NASA software for prediction of acoustic scattering is used to investigate the expected performance of the technology for a range of parameter values. Detailed scattering computational results are presented for several simulated noise sources and for many variations of the Shielding Flap concept. A selection of computational results is compared with experimental data collected in the NASA Langley Quiet Flow Facility. Overall, the results indicate that the Shielding Flap has strong potential to reduce aft-radiated noise, which was a primary design objective, by shielding sound from the simulated sources while also shielding sound that is scattered from the main airframe.

I. Introduction

Community noise of aircraft is significantly influenced by Propulsion Airframe Aeroacoustic (PAA) integration effects, including acoustic reflection, shielding, and diffraction. The net influence, positive or negative, of PAA effects is highly dependent on aircraft configuration. For conventional tube-and-wing aircraft, reflection of engine noise from the wing and fuselage can cause increased noise levels for ground observers as these aircraft fly overhead. For unconventional configurations such as the Hybrid Wing Body (HWB) with engines placed above the airframe, engine noise is shielded by the airframe, thereby reducing noise on the ground. Prior work [1] has shown the noise level difference in an aircraft noise certification scenario due to configuration PAA effects can be as much as 10.7 EPNdB cumulative. However, noise diffracts around the edges of the airframe, which permits some attenuated engine-radiated noise to reach the ground. In addition, jet noise is emitted from the jet plume that can extend downstream of the engine nozzle and the shielding airframe. In all cases, the PAA effects are frequency-dependent and directional. While noise shielding on a HWB configuration can be highly effective at certain emission angles, noise propagated to unshielded angles may dominate certification levels and limit the system-level benefit achieved by the configuration. To drive noise levels even lower, it is necessary to improve the shielding characteristics of the configuration by modifying either the source characteristics (location, directivity, etc.) or the shielding characteristics (planform area, scattering efficiency, etc.).

A NATO task group led by representatives from DLR and NASA was established to assess the acoustic characteristics of an aircraft concept with a hybrid wing body configuration that is representative of a future unmanned combat aerial vehicle. The group was also tasked with developing new technologies and modifications to reduce the acoustic signature of the aircraft. The present paper describes the NASA design of a noise reduction technology termed the Shielding Flap that enhances the innate shielding characteristics of the aircraft concept by further reducing both the edge-diffracted noise and the distributed jet noise. While the concept adds additional shielding area, it also modifies the scattering characteristics to attain more noise reduction compared to a simple planform extension.

In this paper, Section II describes the design requirements and conceptual development of the Shielding Flap. Section III describes a NASA-developed computational tool for the prediction of acoustic scattering that is used to assess the noise reduction potential of the Shielding Flap and the effects of the detailed design parameters that define the device. Section IV presents detailed computational results, first for a simplified two-dimensional airfoil setup, and later for a two-dimensional section of the NATO aircraft concept. Initial comparisons to experimental data are also presented. Finally, conclusions are summarized in Section V.

[1] Research Aerospace Engineer, Aeroacoustics Branch, AIAA Senior Member, ian.a.clark@nasa.gov.
[2] Senior Research Engineer, Aeroacoustics Branch, AIAA Associate Fellow.

II. Shielding Flap Noise Reduction Design

The noise reduction approach focuses on the aeroacoustic effects associated with the propulsion and airframe integration of the MULDICON [2] vehicle. An image of the MULDICON geometry is shown in Fig. 1, where the rectangular nozzle blended with the center body trailing edge of the vehicle is shown. The design requirements stated that the technology should:

- reduce aft-radiated noise,
- prioritize the reduction of scattered turbomachinery noise over jet noise,
- be integrated with the MULDICON vehicle design, although the detailed mechanical design would not be a focus,
- be a deployable device.

In addition, it was desired that essential aeroacoustic effects could be investigated experimentally at a reasonable cost in the NASA Langley Quiet Flow Facility (QFF) using the basic NACA 0012 experimental approach with the laser spark point noise source used previously [3]. The noise reduction was targeted to be primarily in the aft polar angles. This is because achieving noise reduction in these far downstream angles is typically more difficult to accomplish [4]–[6].

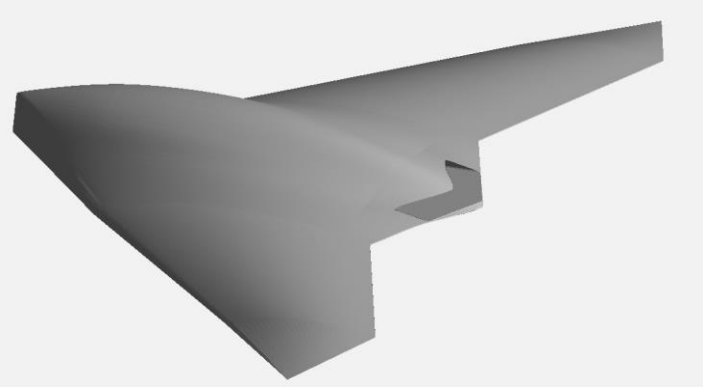

Fig. 1 MULDICON uninhabited combat aerial vehicle design with rectangular nozzle.

A view of the cross-section of the nozzle and trailing edge is shown in Fig. 2. The small horizontal extension of the lower nozzle surface was added by the NATO team to prevent the nozzle jet exhaust flow from deflecting downward because of a Coanda effect. The view in Fig. 2 also shows two primary noise sources, turbomachinery and jet, that will scatter off the trailing edge geometry. While the turbomachinery noise propagates from the exit plane of the nozzle, the jet has a distribution of noise sources extending axially downstream, as indicated by the image. A third noise source is the interaction of the high-speed turbulent jet flow with the trailing edge. In this case, the source of the interaction is in the immediate vicinity of the trailing edge.

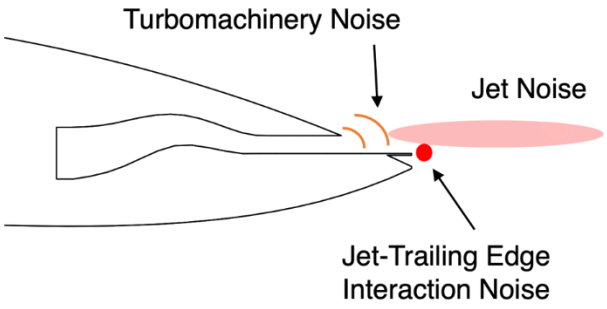

Fig. 2 Cross-section view at the centerline of the MULDICON nozzle and trailing edge.

The most basic addition to the geometry that could reduce turbomachinery noise in the far downstream polar angles would be a simple extension of the lower surface of the jet nozzle. This could also shield some of the jet noise sources. However, it would only move the jet-trailing edge interaction to the new, farther downstream, trailing edge location. The mechanical deployment of this extension, while conceivable, is practically less obvious.

As a result, this simplistic extension concept was rejected in favor of the more complex Shielding Flap concept. The original MULDICON centerline design, the simple Edge Extension, and the selected Shielding Flap concept are all shown in Fig. 3 for comparison. The Shielding Flap introduces several advantages for noise reduction:

- prevention of jet scrubbing on the Shielding Flap such that there would be no additional jet-trailing edge interaction noise,
- would be lower and downstream of the jet-trailing edge interaction so that the Shielding Flap would shield not only turbomachinery noise but also the jet-trailing edge interaction noise and jet noise,
- could easily be a deployable device, stowed in cruise in the underside of the MULDICON and deployed for noise-sensitive parts of a mission at lower speed, low-altitude flight conditions,
- could be utilized for vehicle control or as a speed brake in addition to deployment for noise reduction.

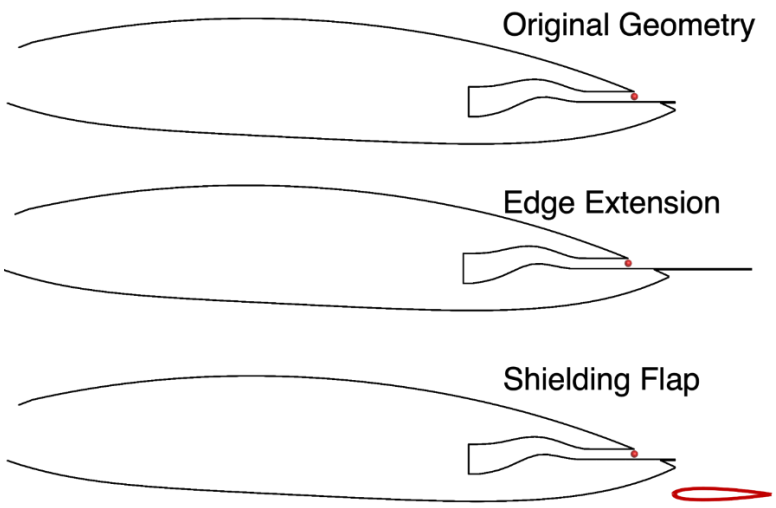

Fig. 3 Side view of the original MULDICON centerline geometry (top), the simplistic Edge Extension concept (middle), and the Shielding Flap noise reduction concept (bottom).

The Shielding Flap is deceptively complex. While it has the advantages listed above, it also introduces additional parameters and physical effects that require investigation, and that makes this a challenging design exercise. These parameters include:

- vertical and streamwise positioning relative to the main-body trailing edge,
- the width of the gap between the Shielding Flap and main body with a nonuniform flow,
- angle of attack that could be positive or negative,
- the cross-section, which could be a flat plate or an airfoil,
- the planform shape of the Shielding Flap, which could have many possibilities and choices.

The refined design objective is summarized notionally in Fig. 4 for the Shielding Flap relative to the more simplistic Edge Extension concept. It represents a tradeoff of less noise reduction in the shadow region (directly under the vehicle where only diffracted noise is observed) but more noise reduction in the downstream polar angles that do not have direct line-of-sound shielding potential. Introducing the gap between the flap and main body creates some leakage of sound into that shadow region under the body and, in turn, there are new parameters, listed above, that can be used in the design to increase noise reduction in the downstream angles.

Much of the essential acoustic physics of scattering effects can still be studied in the NASA Langley QFF with the simplifications of using the NACA 0012 as a surrogate for the MULDICON airframe and with the laser spark as a simplified noise source. This is schematically represented in Fig. 5. Figure 6 shows how essential physics relevant to the Shielding Flap can be experimentally studied, including:

- sharp edge diffraction,
- scattering from multiple bodies (main body and the Shielding Flap),
- effect of the gap flow on upstream scattering,
- effect of the main body and flap boundary layers on scattering.

This represents an additional step to transfer the lessons from the QFF experiment to the MULDICON with realistic turbomachinery and hot jet noise sources.

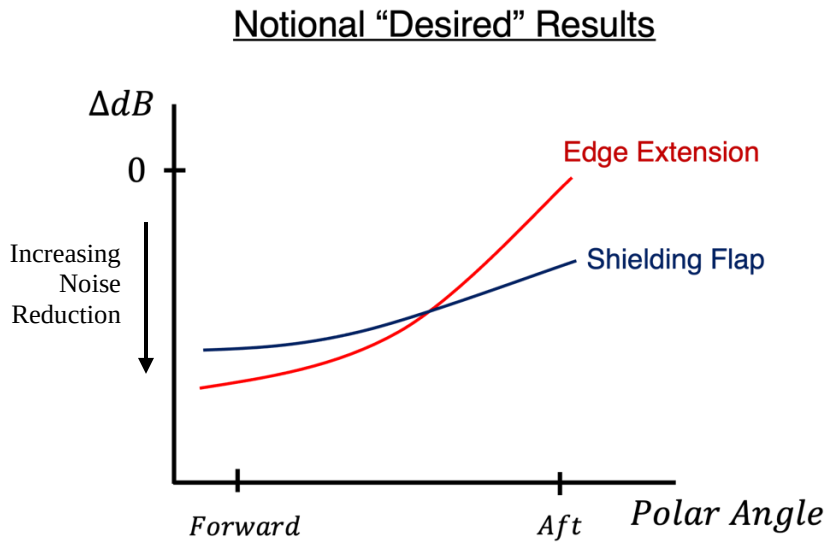

Fig. 4 Notional refined design objective of achieving increased noise reduction in the downstream angles at the expense of some noise reduction directly under the vehicle.

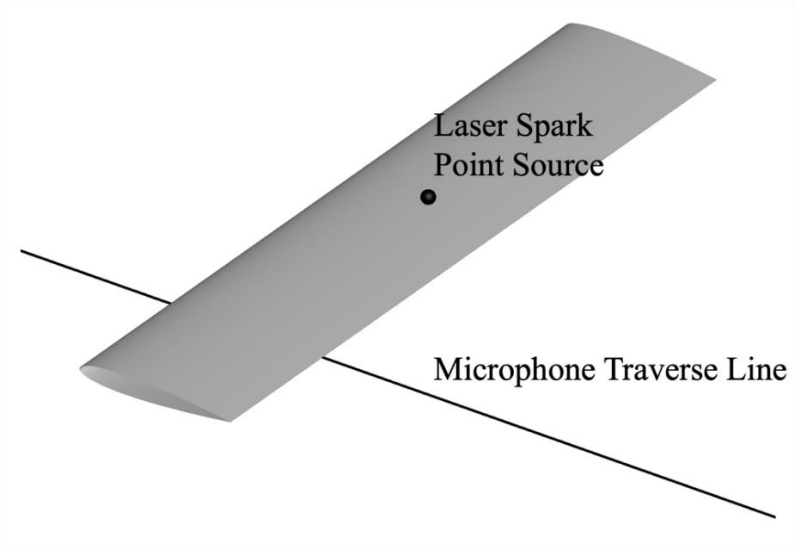

Fig. 5 Simplified schematic of the NACA 0012 airfoil experiment in the NASA Quiet Flow Facility with the laser spark point source to study much of the essential physics for the Shielding Flap concept.

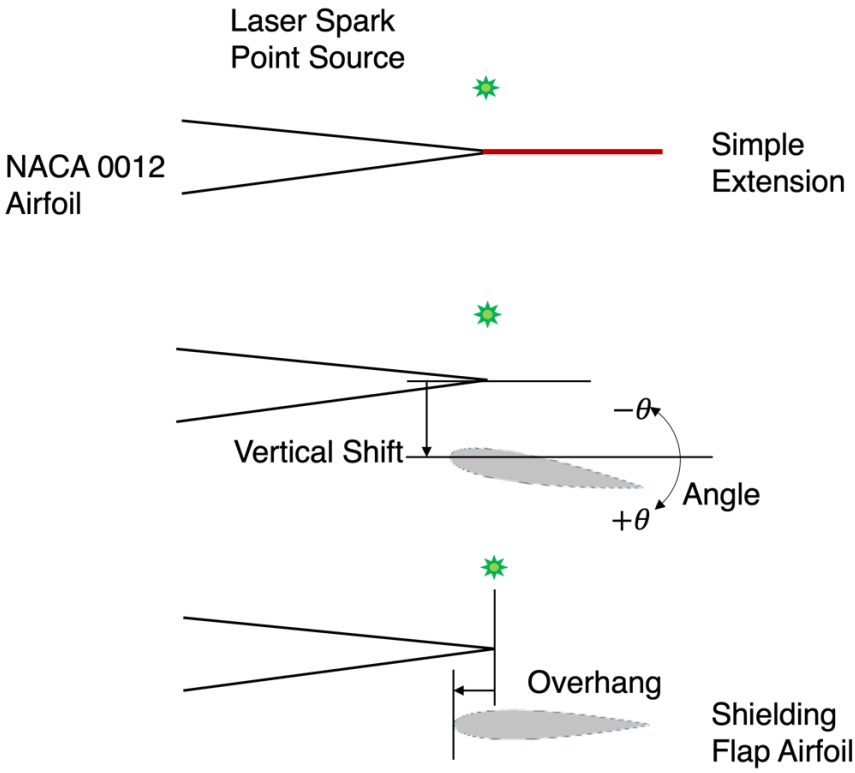

Fig. 6 Schematic of how the NACA 0012 experiment with laser spark source can study many of the essential noise scattering physics relevant to the Shielding Flap concept.

The ultimate implementation of the Shielding Flap concept on the MULDICON is rendered, in end view, in Fig. 7, and in an additional pictorial view, in Fig. 8. Conceptually, therefore, the Shielding Flap meets all design requirements. The real design challenge for the team is to understand the acoustic effects of the parameters and, through experiment and prediction, select the most successful design.

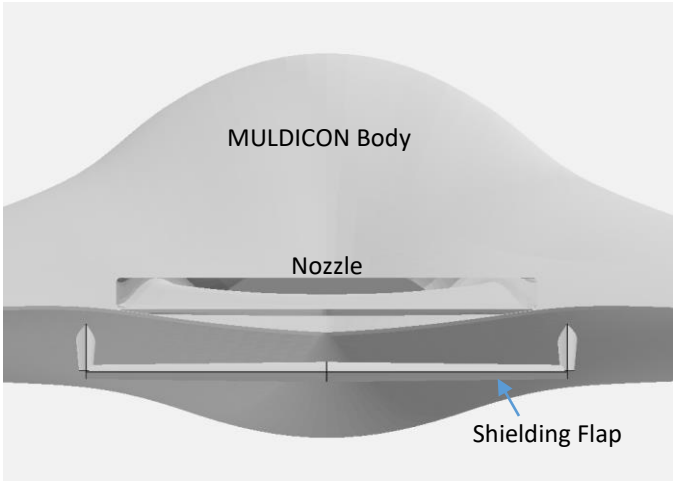

Fig. 7 End view of the MULDICON vehicle with the rendering of the Shielding Flap concept as it would be deployed during a noise-sensitive segment of a mission.

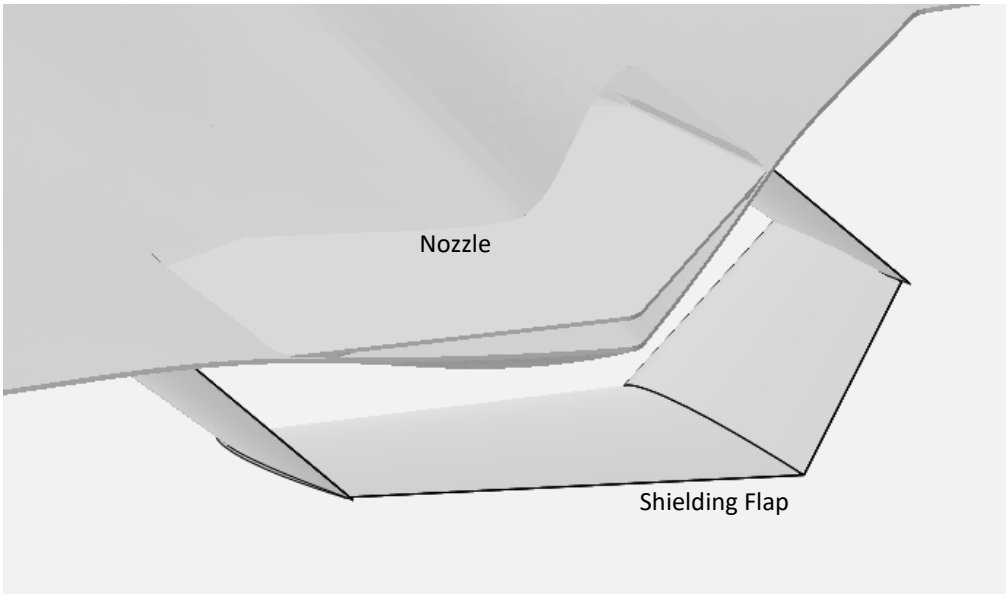

Fig. 8 Rendering of the Shielding Flap noise reduction concept as deployed from the trailing edge of the MULDICON vehicle.

III. Scattering Prediction Methodology

For over two decades, there have been sustained efforts in NASA Aeronautics research to develop prediction approaches for the aeroacoustic effects resulting from propulsion airframe integration, or PAA effects. This is due to three main reasons: the need for more accurate, higher-fidelity aircraft system-level predictions [7], [8], as a new avenue to innovate noise reduction technology [4], [9], and as an integral and necessary tool with which to achieve ambitious noise reduction goals on unconventional aircraft concepts [1], [5], [6], [10]–[13].

For the wide range of applications at NASA, from advanced conceptual aircraft studies to the development of noise reduction technologies or operational procedures for modern aircraft, system-level methods and mid-fidelity computational methods continue to be the most practical and capable way of meeting cycle turnaround time requirements. For many studies, results are needed before the high-quality geometry required for Computational AeroAcoustics (CAA) methods is available. In addition, the aircraft system-level methods provide the best insight into the prioritization of noise sources and interactions [14]. This is helpful at the earliest stages of project planning and technical formulation.

Given the value of predicting PAA effects, several approaches have been investigated with the objective of providing a more capable method compared to the existing WING method in the NASA Aircraft Noise Prediction Program (ANOPP) [15], which is based on semi-infinite barrier theory with an empirical approximation. While the WING method in ANOPP is relatively easy to use and can be used for both shielding and reflection, it is basic in both physics and geometry capabilities. For the NASA PAA and Aircraft System Noise research, and for use with ANOPP, a completely new method has been developed from first principles with grounding in the practical execution of aircraft system noise problems. This method starts with classical geometric acoustics theory. However, for more accurate and robust practical aircraft applications, there are several modifications and extensions in analytical formulations that have been added to the classical theory together with the numerical implementation. This results in a completely new code capable of shielding, diffraction, and reflection prediction, the Propulsion Airframe Aeroacoustic Scattering (PAASc) code. Using only a subset of the PAASc method just for diffraction and shielding prediction, a second code can be used, the Propulsion Airframe Aeroacoustic Shielding Attenuation (PAAShA) code.

The theoretical formulation of the PAASc method has been described in two previous papers [16], [17]. In addition, systematic validation has been presented to demonstrate the applicability, accuracy, and robustness of the method using a wide range of analytical solutions, experiments with canonical geometries [18], experiments of point source scattering by a symmetrical airfoil [3], broadband scattering from a complex aircraft model [19], and scattering from a full-scale aircraft flight test [20]. The method is sufficiently fast in both computation time and total cycle time for

problem setup and processing. For example, for a prediction of scattering from a full-scale Boeing 787-10 aircraft geometry, the computation time for all frequencies is on the order of minutes on a standard desktop personal computer.

Geometric acoustics has been researched extensively in the past and has been applied in various areas in acoustics [21]–[29]. The basic principles of the theory, its limitations, and its favorable features are well documented and discussed. The main limitation is its high frequency asymptotic formulation, limiting its applications to cases where the acoustic wavelength is smaller than the characteristic length scale of the scattering geometry. Despite this limitation, geometric acoustics remains an attractive method in practical applications because of its favorable features, which include its intuitive formulation of rays and ray tubes that closely mimic the physical propagation of sound waves, its ability to accommodate complex surface geometries, and its high computational efficiency. The last is still a critical requirement for practical aircraft noise applications even with the drastic improvements of computing power of modern computers in recent years. It is orders of magnitude more efficient than any other numerical method, such as the volume discretization method of Computational Aeroacoustics (CAA) and the surface discretization method of the Boundary Element Method (BEM). It is the only known method feasible for quick turnaround engineering applications of full configuration aircraft for the most important frequencies in the kilohertz range. Because of this, geometric acoustics has attracted attention in recent years for aircraft noise applications [30]–[35]. A key to the effective use of geometric acoustics in aircraft noise scattering, however, is not a simple matter of straightforward application. Rather, the basic theories need to be modified and extended to account for the unique features of complex aircraft noise sources, effects, and geometric features.

The method developed and implemented in the NASA PAASc code has demonstrated excellent validation results. For reflection, some examples have been reported [16] to illustrate the accuracy, and more importantly, to demonstrate the effects of key features. These have included the importance of curved surface reflection in comparison with analytical solutions and the approximation of panel reflection. The agreement between the analytical solutions and the formulation for curved surface reflection is very good and far superior to the panel reflection approximation, which greatly overpredicts the interference between the incident and the reflected waves, leading to large errors. The importance of source coherence in sound scattering calculations has been demonstrated with comparisons between the coherent and the incoherent calculations, together with comparisons to wind tunnel test data.

A systematic validation of the diffraction and shielding methodology in PAASc (and PAAShA) has been reported [17] for progressively more complex problems and experiments that are representative of aircraft-like applications. Comparisons have been reported for geometries of increasing complexity and for a variety of sources from multiple experiments and facilities. In some cases, comparison was made with analytical solutions. Over this wide range of problems, geometries, and sources, the method was proven to be robust and efficient. Accuracy is typically 1–4 dB (and often on the lower end of this range) over a wide range of the most significant frequencies and directivity angles. Accuracy can be somewhat diminished for high azimuthal directivity angles, often of less relevance. It should be noted that experimental data have their own uncertainty related to resolution in frequency, angle, and source characteristics (size, shape, spectrum, etc.).

IV. Numerical Analysis

NASA numerical analysis focuses on the design of the Shielding Flap to optimize noise reduction and follows a progressive process of parametric studies using the PAASc prediction capability. The design process starts with the simple geometry of a baseline NACA 0012 airfoil with Shielding Flaps, then proceeds to a two-dimensional cross-section model of the MULDICON concept with Shielding Flaps. A design of the Shielding Flap for the full three-dimensional MULDICON configuration has not been completed.

A. NACA 0012 Airfoil

The design using the basic NACA 0012 airfoil is coordinated with the experimental effort in the NASA QFF, with the numerical analysis conducting many parametric computations to select the most promising configurations for the QFF tests. The computational setup consists of the same layout and dimensions as in the tests with the NACA 0012 airfoil and the Shielding Flaps. The measurement locations are distributed along a line in the flow direction, at the midspan and on the shadow side of the airfoil one chord length from the airfoil centerline. The measurement locations extend from two chord lengths of the main airfoil upstream of its leading edge to two chord lengths downstream of its trailing edge. The geometry is illustrated in Fig. 9. The airfoil has a chord length of 200 mm and a trailing edge thickness of 0.254 mm. The source is assumed to be a coherent point monopole source and can have five positions. In the flow direction, the five positions are at 0%, 50%, 70%, 75% and 100% of the main airfoil chord length, measured from its leading edge, and the source positions are 25 mm above the airfoil surface, except for the one at the 70% chordwise location that is 40 mm from the surface. In Fig. 9, the source shown is at 70% of the airfoil chord length

from its leading edge. The design parametric computations are done with three values of the mean flow Mach number: 0.00, 0.13 and 0.16. However, the results are presented for static medium because the effects of the mean flow may change the quantitative results but not the qualitative conclusions that are the basis of the design optimization.

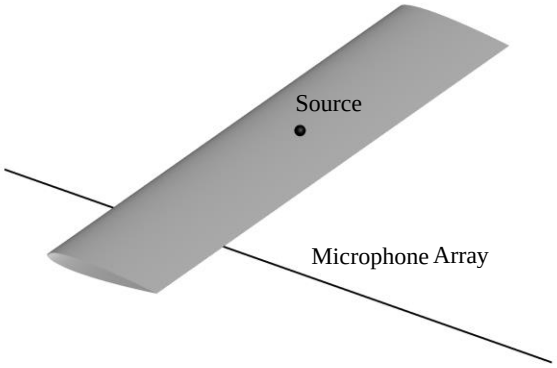

Fig. 9 Illustration of computational setup for NACA 0012 flap design.

Two types of Shielding Flaps are used in the computations, one being a flat plate and the other a NACA 0015 airfoil. Both have a chord length of 25.4 mm and a trailing edge thickness of 0.254 mm that is the same as the trailing edge thickness of the main airfoil. For each type of flap, three parameters are varied: the flap overhang in relation to the trailing edge of the main airfoil, the shift of the flap toward the microphone side, and the flap angle, defined positive when the flap is rotated toward the microphones, all shown schematically in Fig. 6. The values of these parameters are given in Table 2, together with the values of other parameters to show the complete computation matrix.

Table 2 Computational matrix for the NACA 0012 airfoil with Shielding Flap.

Parameter	Values
Source Position (%)	0, 50, 70, 75, 100
Mach Number	0, 0.13, 0.16
Flap Type	Plate, NACA 0015 Airfoil
Overhang (mm)	-6.35, 0, 6.35, 12.7, 19.05
Shift (mm)	0, 3.175, 6.35, 9.525, 12.7, 15.875, 19.05
Flap Angle (Deg)	-10, 0, 10

From this large computational matrix, a subset of configurations, which are shown in Fig. 10, is selected for presentation of results and analyses. There are two types of flaps with three flap positions: an extension position with the flap attached to the main airfoil, a gapped position where the flap is moved in the downstream direction to create a gap of 6.35 mm between the trailing edge of the airfoil and the leading edge of the flap, and a shifted position with the flap shifted toward the microphones by an amount of 6.35 mm.

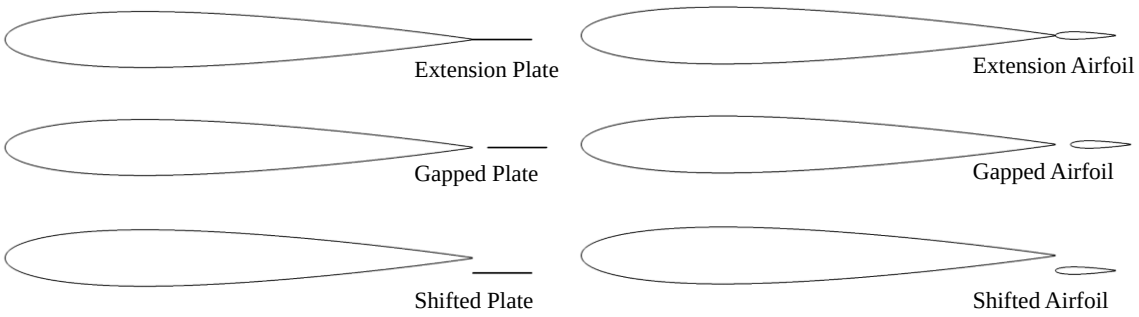

Fig. 10 Configurations for Shielding Flap computation with the NACA 0012 main airfoil.

The effects of the extension flap on noise shielding are shown in Fig. 11, where the ΔSPL on the vertical axis is the sound pressure level for the scattering case minus that for the isolated source, showing the shielding effects as negative values, and the horizontal axis is the coordinate in the flow direction normalized by the chord length of the main airfoil. Thus, the leading edge of the main airfoil is at zero and its trailing edge is at one. For comparison, the results for the main airfoil alone are also shown in the plots. Since the flaps in these cases effectively increase the chord length of the scattering geometry, the results and physics of the scattering are simple. The extension flaps simply move the trailing edge diffraction to a different location further downstream. The overall amplitudes at the upstream microphone positions (upstream of the midchord of the main airfoil) are basically the same, because this spatial range is dominated by the diffraction from the main airfoil leading edge, which is the same for all three cases. The shift of the dips and peaks in this range from the case of the main airfoil alone to the cases of extension flap is due to the changes from the trailing edge diffraction, which is more clearly shown in the downstream range of the results. Here, the extension flap increases the shadow region and lowers the noise amplitude from the case of the main airfoil alone at fixed locations. The difference between the extension plate and the extension flap in this spatial range is due to the diffraction from different trailing edge angles.

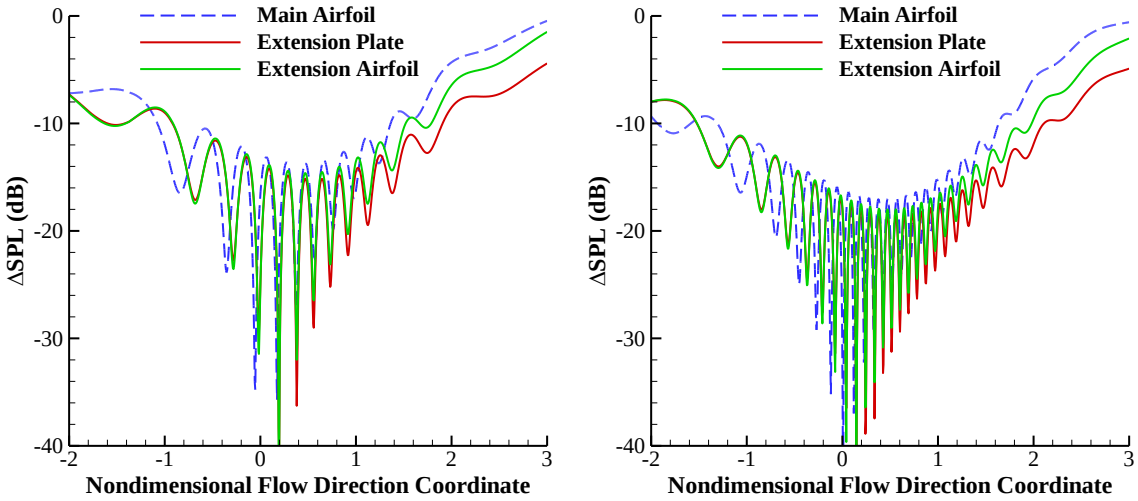

Fig. 11 Effects of extension flap on noise shielding for 10 kHz (left) and 20 kHz (right).

For the gapped flaps, the edge diffraction occurs at four edges, which follow the same diffraction physics, with the gap allowing the diffracted noise to reach the shadow and the partially insonified regions. Thus, an increase of noise in some spatial range is expected. This is indeed confirmed by the results shown in Fig. 12, where the noise in the region close to and slightly downstream of the trailing edge of the main airfoil is higher than in the case of the main

airfoil alone, due to the combined effects of multiple edge diffraction and gap leakage. The gapped airfoil flap suffers more leakage of noise into the shadow region and the partially insonified region, in comparison with the gapped plate flap, because there is more scattering off the smooth leading edge of the flap.

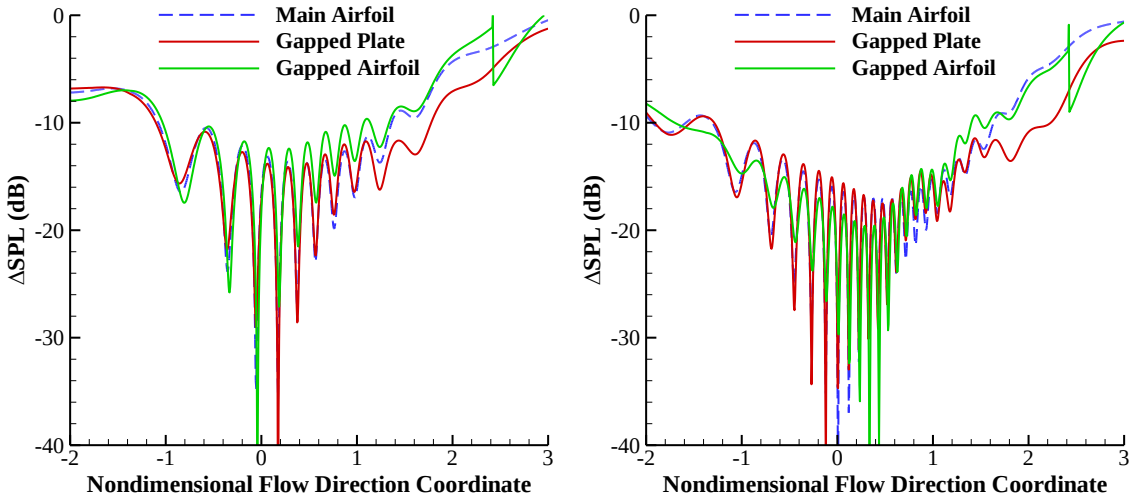

Fig. 12 Effects of gapped flap on noise shielding at 10 kHz (left) and 20 kHz (right).

When the flaps are shifted toward the microphones, the noise reduction due to shielding is increased in the region downstream of the main airfoil trailing edge, as shown in Fig. 13. Upstream of the main airfoil trailing edge, the flaps do not block the edge diffraction so that the main airfoil scatters the noise in the same way as an airfoil without a flap, leading to almost identical results in this region for all three cases shown in the figure.

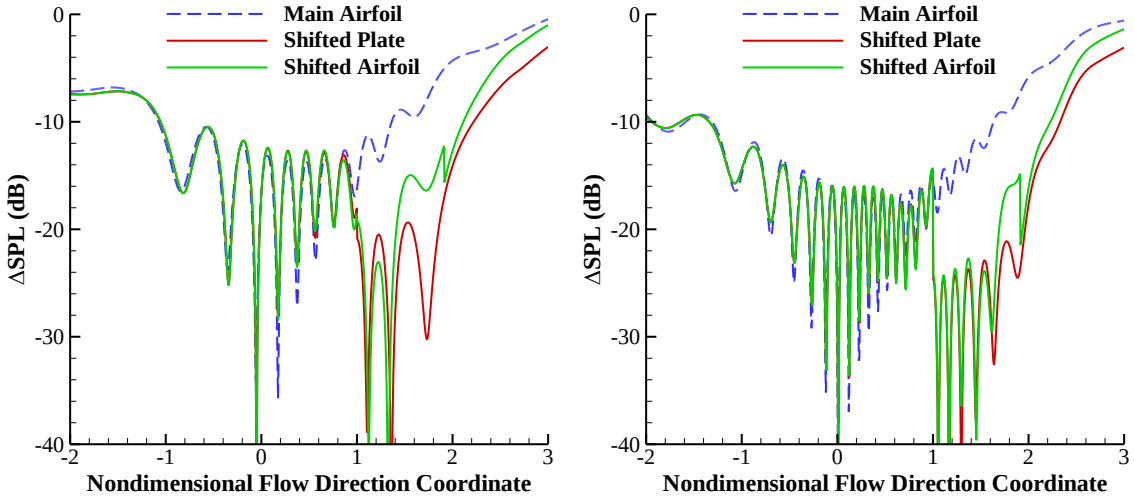

Fig. 13 Effects of shifted flap on noise shielding at 10 kHz (left) and 20 kHz (right).

The shifted flap configuration results in a noise reduction downstream because the flap blocks the diffraction from the main airfoil trailing edge, which is a major contributor of noise in this region. With this blockage, the noise in this region mainly comes from the trailing edge of the flap, which is weaker than the main airfoil trailing edge diffraction or that of the extension flap connected to the main airfoil, because of the smaller dimension of the flap when it is not connected to the main airfoil. The scattering physics is illustrated in Fig. 14. For an extension flap, the flap effectively

increases the dimension of the scattering geometry by 1/8 of the main airfoil chord in this case. Thus, the relative diffraction strength can be regarded as 9 units, or as being unchanged at 8 units from the baseline airfoil if the total chord is much larger than the wavelength so that the diffraction is within the limit of geometric acoustics. This strength is proportional to the noise diffracted to the far field. In comparison, when the flap is not connected to the main airfoil, the total diffraction strength of 9 units is divided between the main airfoil and the flap, approximately 8 units and 1 unit, respectively, because the flap chord is smaller than the wavelength, and thus has not achieved the strength of geometric diffraction. For the shifted flap, the diffraction proportional to 8 units is blocked by the flap and the remaining noise to the far field is only proportional to one unit, a much weaker contribution. The method of geometric acoustic diffraction cannot capture this low frequency, or large wavelength, feature. The method in PAASc has a correction to account for this based on the diffraction physics.

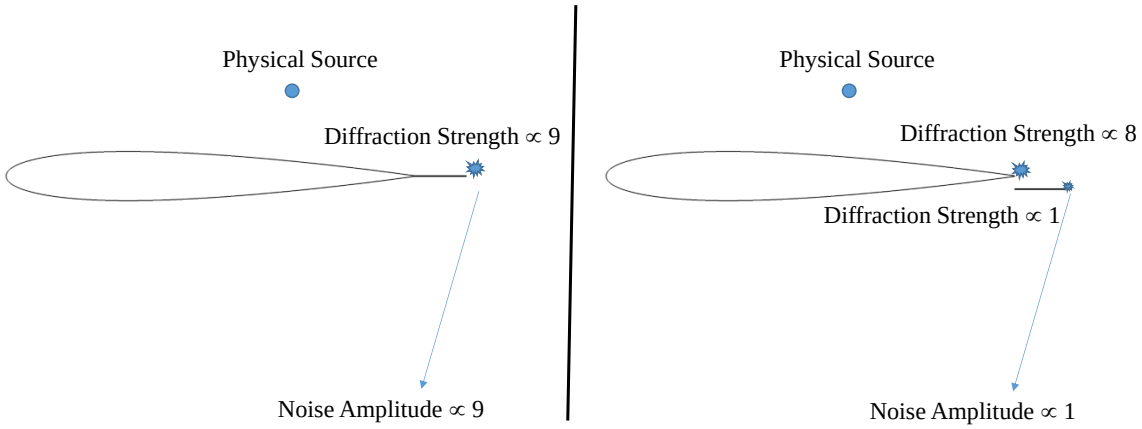

Fig. 14 Illustration of diffraction physics for extension flap and shifted flap.

The results given in this section are a subset of the large matrix of parametric studies designed to select the best potential Shielding Flap configuration for noise reduction. The parametric studies involve all combinations of the parameters listed in Table 2, for a total of 3150 configurations. From the parametric studies, all Shielding Flap configurations have been shown to be effective in reducing noise, in comparison to the baseline airfoil, by increasing the shadow zone. This is intuitive because the flap increases the dimension of the scattering geometry. However, the additional noise reduction from the baseline and between the flap configurations is not uniform in space and frequency. This is because the additional noise reduction can be partially or completely offset by some features of the individual configurations in certain space and frequency ranges. The leakage from the gap between the flap and the main airfoil is an example. Because of this, the noise levels can revert to the baseline levels at some angles. Across the studied configurations, the shifted flap with zero or positive angle and a small overhang seems to be the best configuration. It extends the shadow zone in the same way as other configurations, which is the most beneficial feature of Shielding Flaps, but has the extra benefit of blocking the propagation from the source to the microphones through the gap, minimizing the gap leakage of the diffraction by the flap leading edge, and shielding the diffraction from the main airfoil trailing edge. Although the flat plate appears to have a small advantage in shielding, practical flow considerations would highly favor an airfoil in application.

The noise reduction potential by Shielding Flaps is most beneficial in the aft quadrant downstream of the main airfoil trailing edge. This region covers a portion of the shadow region and a portion of the partially insonified region. In aircraft noise shielding, because the engines are usually located near the trailing edges, noise shielding in the aft quadrant is usually not efficient. Thus, additional methods such as a Shielding Flap may be needed to help achieve greater noise reduction. The airfoil/flap geometry studied in this section is not meant to simulate any realistic vehicle, but rather to build understanding of the relevant physics and establish noise reduction trends with design parameter variations. The scattering effects of a vehicle are highly dependent on the scattering geometry as well as the source location, which is why the design process is planned to progress toward the MULDICON geometry. An intermediate step is described in the next section.

B. MULDICON Cross-Section Model

As an intermediate step before the design of Shielding Flaps for the full configuration MULDICON vehicle, a cross-section model is considered for parametric studies, which uses the midspan cross-section to construct a spanwise-invariant geometry. The measurement locations for the computations are on a 10-meter radius arc, illustrated in Fig. 15. The arc is on the lower side of the vehicle and its center is at the origin of the coordinate system for the scattering geometry, which is chosen to be the leading edge of the vehicle. The polar angle is defined such that the upstream direction is at zero degrees.

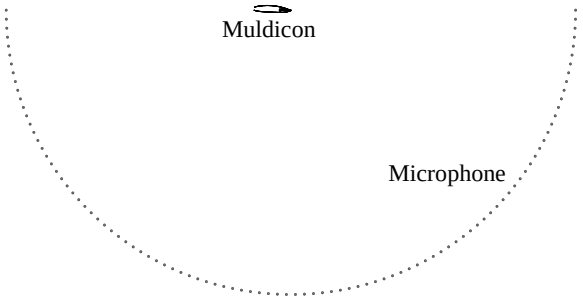

Fig. 15 Illustration of microphone positions for computations of the cross-section MULDICON model.

The scattering geometry is shown in Fig. 16, together with four configurations used in the computations. The first is the baseline MULDICON geometry. The second is a simple extension plate attached to the lower edge of the exhaust nozzle. The third is a group of positions for a NACA 0015 flap with its leading edge fixed at a position inside the cavity formed by the nozzle plate and lower fuselage surface, with the flap angle at -10, 0, and 10 degrees. The fourth is also a group of positions with the flap leading edge shifted away from the nozzle flow and flap angle at three positions. The length of the extension plate and the chord of the flap are both 25.4 mm, 1/8 of the MULDICON centerline chord.

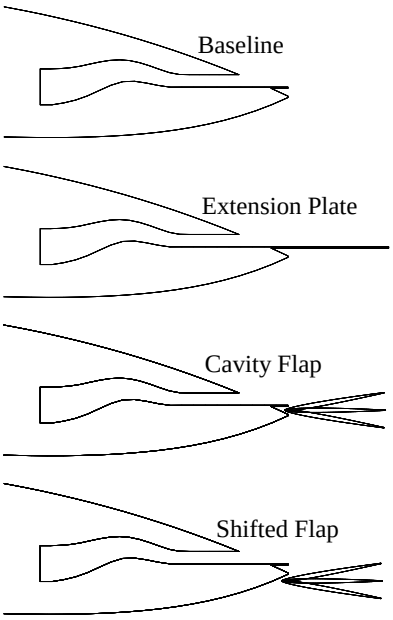

Fig. 16 Flap configurations for MULDICON.

The sources are defined to model both the fan noise and the jet noise sources in the nozzle flow. The source locations are illustrated in Fig. 17 for both the baseline geometry with or without flaps (upper plot) and the extension plate (lower plot) geometry. The fan noise source is modeled as a coherent source located at the exit plane of the nozzle. Three point sources are used to model the jet noise sources, all incoherent. The source at the lower trailing edge of the nozzle or the extension plate represents the interaction source between the jet flow and the trailing edge. The two other incoherent sources approximate the distributed sources in the jet plume, one at half flap chord and the other at one flap chord downstream of the trailing edge.

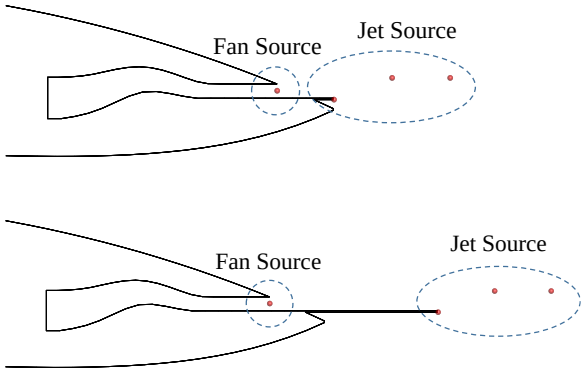

Fig. 17 Source locations for baseline/flap (upper) and extension plate (lower) geometry.

Though the cross-section model cannot capture the three-dimensional scattering of the full configuration MULDICON, it includes some features that are absent in the airfoil model discussed in the previous section, which may have significant impact on the scattering characteristics. In the trailing edge region, there are multiple edges. The nozzle has lower and upper edges that are not aligned. Below the lower nozzle edge, there is potentially a cavity, providing another edge for diffraction. The geometry has a thick curved body upstream of the trailing edge region, potentially acting as a shielding body to upstream angles. The sources for the MULDICON vehicle are different from those of the airfoil case. The fan noise source is very close to the scattering surface, from which efficient shielding can be expected, while the jet noise sources are mostly downstream of the geometry with at least partial direct radiation from the sources to the microphones. The jet noise sources are incoherent so that no interference pattern is expected in the scattered noise. There are altogether 96 configurations covering the parameters discussed in the previous paragraphs, which is much fewer than the 3150 cases for the NACA 0012 airfoil computations. Because some parametric variations are not included here, such as the gap width and the flap overhang, the selections of these parameter values will partially rely on the results and analyses of the NACA 0012 computations.

The shielding effects on the fan noise component at 20 kHz due to the cavity and shifted flaps are shown in Fig. 18. In both cases, the shielding ΔSPL is plotted as a function of the polar angle. The baseline and the extension plate are also shown in the plots for comparison, represented by the red and the green curves, respectively. For both groups of flaps, results for all three flap angles are shown in the figure.

The baseline configuration shows good shielding on the fan noise because the lower trailing edge of the nozzle is many wavelengths downstream of the source, so most of the polar angles under consideration are in the shadow region. For angles larger than 90 degrees in the aft quadrant, the shielding provides up to 20 dB noise reduction with the noise mostly from the weak diffraction at the lower trailing edge of the nozzle. In the forward quadrant with angles smaller than 90 degrees, the noise reduction is further enhanced by the blocking of the trailing edge diffraction by the lower edge of the cavity and by the highly curved lower body surface upstream of the cavity. Since the blocking occurs only for angles less than 90 degrees, the enhanced noise reduction has a sudden drop at this angle, as shown in Fig. 18. In the blocked region, the noise shielding can be as much as 40 dB for the fan noise component. A source of uncertainty in the computation and results for the baseline configuration is the size of the cavity. If the opening of the cavity is smaller than a wavelength, its lower edge cannot be treated as an independent scattering feature because the sound waves cannot distinguish it from the lower trailing edge of the nozzle. In this case, the shielding will be given by the trailing edge diffraction without any blocking and the fan noise reduction will be on the order of 20 dB, still an impressive amount of noise reduction for the baseline configuration without any added shielding device.

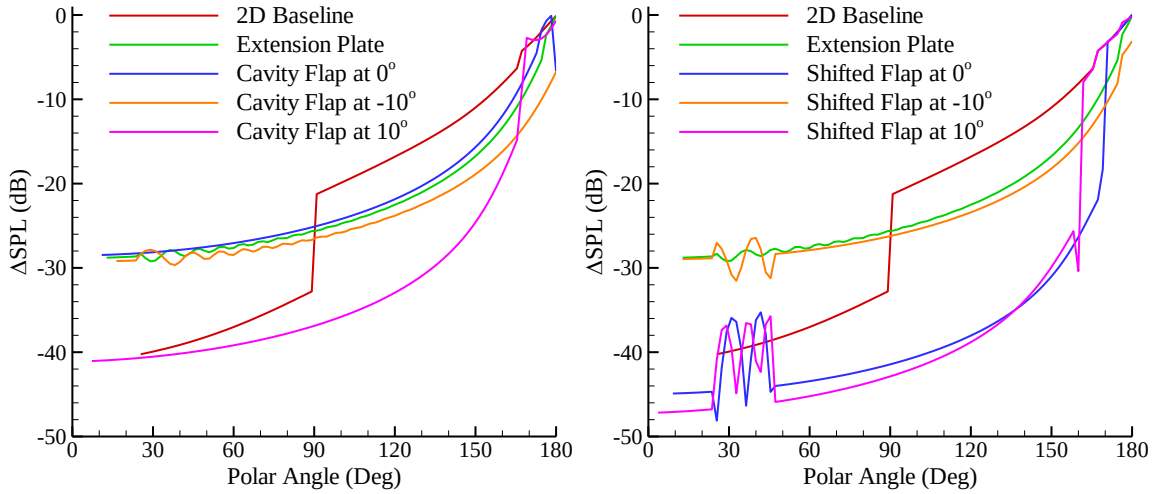

Fig. 18 Shielding effects on fan noise at 20 kHz by cavity flap (left) and shifted flap (right).

For the configuration with an extension plate, represented by the green curves in Fig. 18, an increase in the noise reduction is observed in the aft quadrant with a decrease in the noise reduction in the forward quadrant relative to the baseline. As analyzed in the previous section for the NACA 0012 airfoil, the attached plate expands the shadow region and enhances the shielding effect, which is the reason for the increased noise reduction in the aft quadrant shown in the figure. This mechanism also applies to the forward quadrant, but the extension plate, with its trailing edge further downstream, also eliminates the blocking by the lower edge of cavity. The combined effects of these two features are some noise increases in the forward quadrant. These noise increases, however, are not considered a concern because the noise levels in this region are already very low.

By comparing the results of all the flap configurations plotted in Fig. 18, the shifted flap with zero or positive deployment angle appears to be the best in maximizing the shielding effect for aft fan noise, which is consistent with the conclusion from the parametric studies for the NACA 0012 airfoil discussed in the previous section. The scattering mechanisms resulting in the best shielding effects are similar for the two cases. For the MULDICON case, the main benefit comes from the blocking of the diffractions from the lower trailing edge of the nozzle and the lower edge of the cavity. Because of the presence of a gap between the main body and the flap, there is some leakage effect directed at small angles in the upstream direction leading to some noise increase in the region between about 20 to 50 degrees, as shown by the right plot in the figure.

The jet noise for the MULDICON vehicle has a component resulting from the interactions between the jet flow inside the nozzle and the lower trailing edge of the nozzle. The source location of this noise component is close to the trailing edge. Thus, an incoherent source at the trailing edge is used to model the edge noise, with the results given in Fig. 19 at 20 kHz for the cavity and shifted flaps. The results for the baseline and the extension plate are also given in the figure. For the baseline, the noise from the edge source is shielded by the MULDICON body in the forward angles from the trailing edge, which leads to the gradual increase in noise reduction, up to about 10 dB, as the polar angle decreases, shown in the figure by the red curves. In aft angles, the microphones have direct line of sight to the source so that the shielding is zero. The shielding effects for the baseline geometry start at about 120 degrees in polar angle because the coordinate system is based on the leading edge of the vehicle. The extension plate does not help the shielding of the edge source at all. The plate effectively shifts the source location further downstream away from the scattering body, which gives zero shielding for all angles, as shown by the green curves in the figure.

Since the source of the jet/edge interactions is at the lower trailing edge of the nozzle, all flap configurations help to significantly enhance the shielding effects by blocking the direct radiation from the source to the microphones and by blocking the diffraction from the lower edge of the cavity in the case of the shifted flaps that are located below the cavity. The flaps are similarly efficient in shielding except for the shifted flaps in a small angular range in the forward direction, from about 20 to 50 degrees, where the leakage from the flap gap leads to some noise increase. There are some variations in the shielding level as a function of the flap angle, with negative angles better than positive angles, especially in the aft directions in the partially insonified region. This is because negative angles increase the shadow region and positive angles reduce the shadow region. The negative flap angles, however, are not recommended for

practical applications because the flap trailing edge is likely to intrude into the jet plume, inducing additional noise sources that may reduce or cancel the shielding effects.

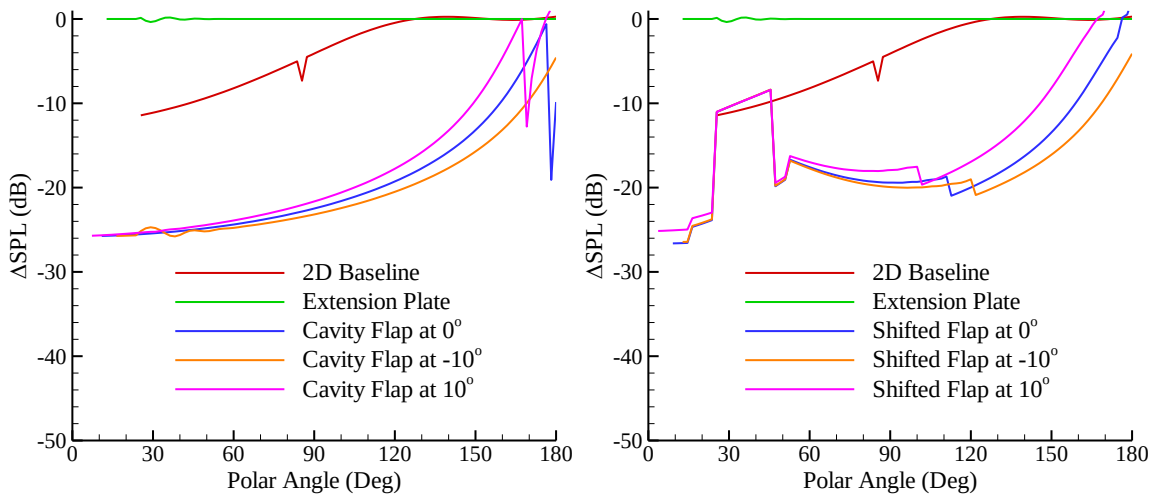

Fig. 19 Shielding effects on jet/edge interaction noise at 20 kHz by cavity flap (left) and shifted flap (right).

The jet noise also has a component from sources in the jet plume, which is modeled in this work by incoherent point sources located some distance downstream of the nozzle trailing edge. The shielding effects for these sources are shown in Fig. 20 for all the flap configurations with the source at the half flap chord location. In this case, the baseline and the extension plate have limited shielding effects, only a few dB in the forward angles. Similar to the case of edge sources, the flaps are similarly efficient in shielding except for the shifted flaps in a small angular range in the forward direction where the leakage from the flap gap leads to some noise increase, and the leaked noise levels are limited by the baseline levels. Also similarly, negative flap angles seem to give more shielding, but this should not be considered a practical configuration because of the potential of jet/edge interaction, as discussed in previous paragraphs.

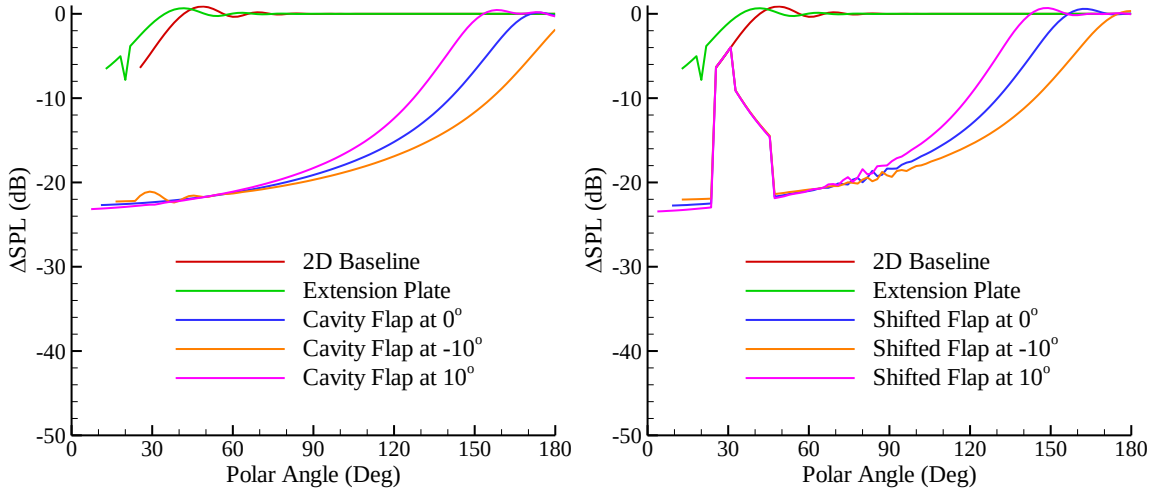

Fig. 20 Shielding effects on jet noise from near edge source at 20 kHz by cavity flap (left) and shifted flap (right).

For jet noise generated by sources in the jet plume far downstream of the nozzle, an incoherent source is used, and its location is chosen to be one flap chord length downstream of the lower trailing edge of the nozzle. The shielding

effects are shown in Fig. 21. In this case, there is no shielding attained for either the baseline and the extension plate configurations, shown by the red and green curves, respectively, because the source is far away from the scattering body. When a flap is added to the baseline, the flap extends the scattering body in the downstream direction, and the flap trailing edge is close enough to the source to have some shielding effects, even though the noise reductions are smaller than those for other sources discussed earlier in this section. The shielding characteristics are essentially determined by the flap trailing edge, with noise reduction starting at the boundary of the shadow zone and gradually increasing into the shadow zone as the polar angle decreases. It is interesting that for this source location, a flap with a negative angle gives less shielding in comparison with other angles. This is opposite behavior compared to other source locations discussed earlier in this section. This is because the source is aligned with the flap trailing edge at the zero-degree position in the flow direction, and a negative angle reduces the shadow region, and thus reduces the shielding effects.

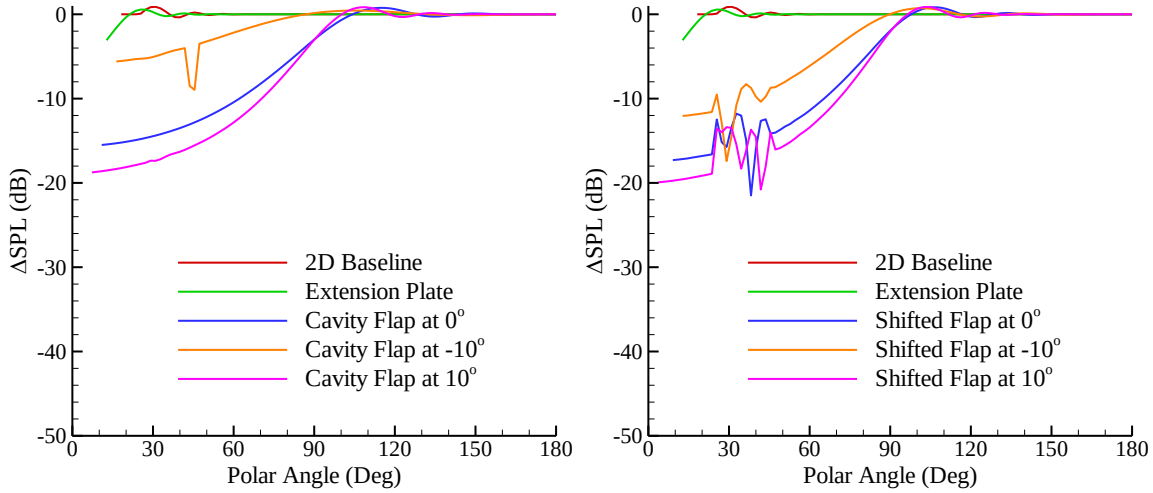

Fig. 21 Shielding effects on jet noise from downstream source at 20 kHz by cavity flap (left) and shifted flap (right).

From the results and analysis presented in this section, the best Shielding Flap for the MULDICON vehicle seems to be the shifted flap with zero or positive flap angle and with a small positive overhang. This configuration gives the best shielding benefit in the widest frequency and spatial ranges for both the aft fan noise and the jet noise from the nozzle. It also has advantages in practical applications, such as avoiding jet/flap interactions.

It is important to emphasize that the computations are not simulations of the real MULDICON vehicle. The geometry is simplified as a cross-section model and the sources are modeled as simple ideal sources. Three-dimensional scattering is not captured in the results presented here. Improvements to the calculations can be achieved by using distributed sources with realistic directivity, which is known to significantly affect scattering. For these reasons, the results presented here should be considered as representing qualitative trends, instead of quantitative effects.

C. Comparison with Experimental Data

From the analysis of the QFF test data, it is shown that the coherent source and the multiple propagation paths lead to scattering patterns that are dominated by rapid variations in sound pressure levels in both frequency and spatial domain, taking the form of sharp dips and peaks as seen in Fig. 22. This makes it difficult to analyze the scattering effects and to compare results both between configurations and between predictions and data when considering a single frequency and a single measurement point. Future work will consider integration, weighting, and/or normalization to develop metrics to assess the shielding efficiency and to compare data with predictions, but the present work will utilize comparisons based on the single frequency and single measurement point results. The quantity in the figures in this section is sound pressure level for exact frequencies in the computations and for frequency bands of 61 Hz in the data.

For the case of an extension plate attached to the baseline NACA 0012 airfoil, examples of the comparisons between data and predictions are given in Fig. 22. These results correspond to static conditions with the source at 70%

airfoil chord length. There are discrepancies between data and predictions, some of which are also seen in other cases, as will be presented later in this section. The reasons for these discrepancies, either due to mismatch of configurations and conditions between tests and computations, or due to inadequate modeling in the computations of some aspects of the scattering process, or both, will be discussed later in this section.

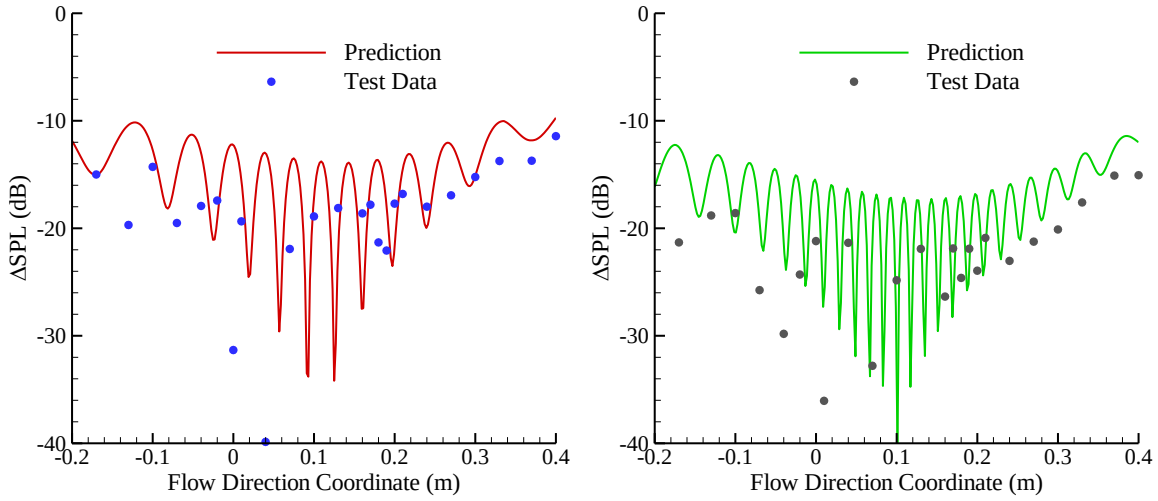

Fig. 22 Comparisons between test data and predictions for extension plate at 10 kHz (left) and 20 kHz (right) for M=0 and the 70% source position.

If the comparisons are made between the curves and the trends formed by the symbols, the discrepancies seem to be very large. These kinds of comparisons, however, can be misleading because the measured data are sparsely distributed and simple linear interpolation between data points for coherent sources are known to be inaccurate if the data points are far apart from each other, as is the case here. The distances between the data points are usually larger than the period of variations, as is clear from the figure, and thus, the sharp dips and peaks are likely missed by the measurements. In fact, many data points are right on or close to the prediction curves, indicating accurate prediction at these locations. There are some low-level data points that are far below the prediction. If the flow direction coordinates of these points are aligned with or close to any sharp dips on the curves, the discrepancies are not prediction errors of concern, but due to the sensitive nature of the dips to the precise measurement location and the precise value of the coherence, both of which are not exactly matched between tests and computations. These considerations should be applied to all the comparisons in this section.

For flaps shifted from the main airfoil chord line toward the microphone side by the amount of 12.7 mm, comparisons are given in Figs. 23 and 24, for flap angles of zero and -10 degrees, respectively. For shifted flaps, an important feature predicted by the computations is the noise reduction in the downstream direction in comparison with both the baseline and the extension plate case, approximately between x=0.2 m to x=0.35 m, downstream of the trailing edge of the main airfoil. These predicted lower noise levels are indeed measured in the tests, as shown in the two figures, but there are significant discrepancies in the details, such as a smaller range of the low noise region in the data than in the predictions. The reasons behind this discrepancy will be discussed at the end of this section. The comparisons for the region upstream of the main airfoil trailing edge are reasonable good, with the majority of the test data falling within the expected range of the dips and peaks predicted by the computations. The negative flap angle leads to changes in the scattered noise, both in the test data and in the predictions, as is clear by comparing the two figures. Since the focus for these figures is the comparisons between data and predictions, the meaning and the scattering physics of these changes will not be analyzed here. In terms of comparisons, the agreements and discrepancies are similar between the cases of zero and negative flap angle.

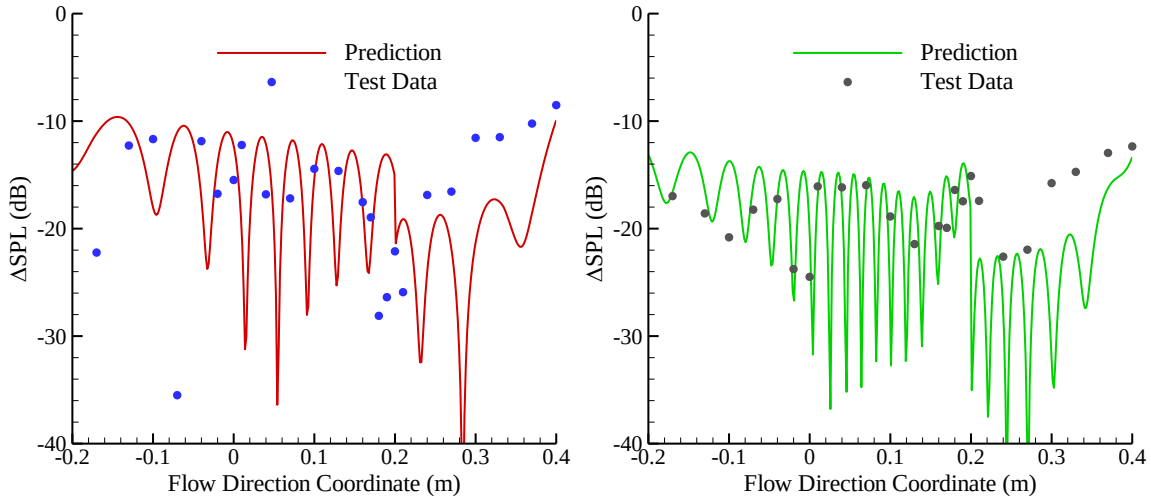

Fig. 23 Comparisons between test data and predictions for shifted flap at zero angle and zero overhang for 10 kHz (left) and 20 kHz (right) for M=0 and the 70% source position.

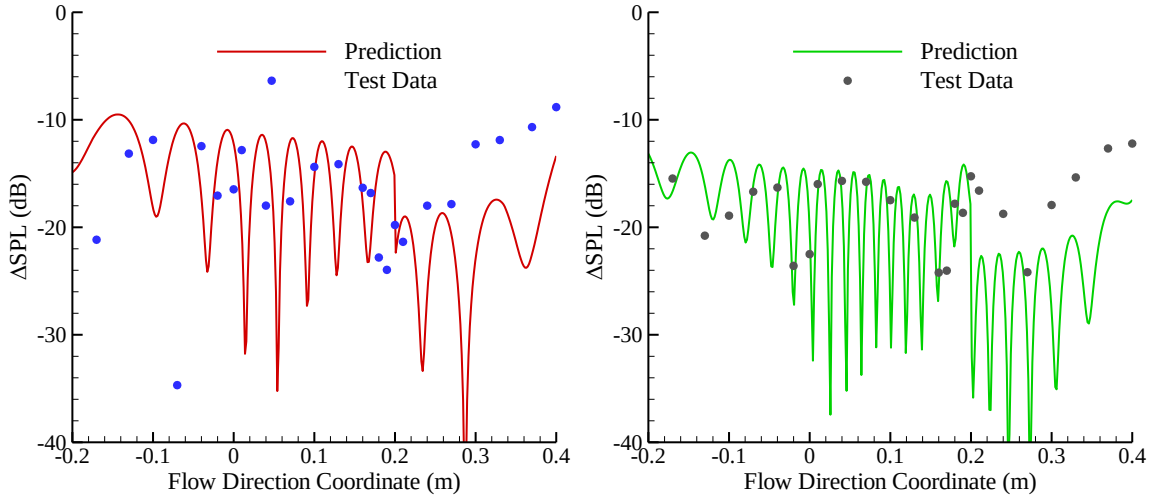

Fig. 24 Comparisons between test data and predictions for shifted flap at -10 degrees angle and zero overhang for 10 kHz (left) and 20 kHz (right) for M=0 and the 70% source position.

For shifted flaps with positive overhang of 6.35 mm, some comparisons are given in Figs. 25 and 26 for flap angles of 0 and -10 degrees, respectively. The flap overhang is designed to modify the scattering by reducing the leakage from the gap between the flap and the main airfoil. The assessment of this concept is not the focus of these two figures and thus will not be discussed here. For the comparisons between data and predictions, the overall trends of agreements and discrepancies are similar to other configurations.

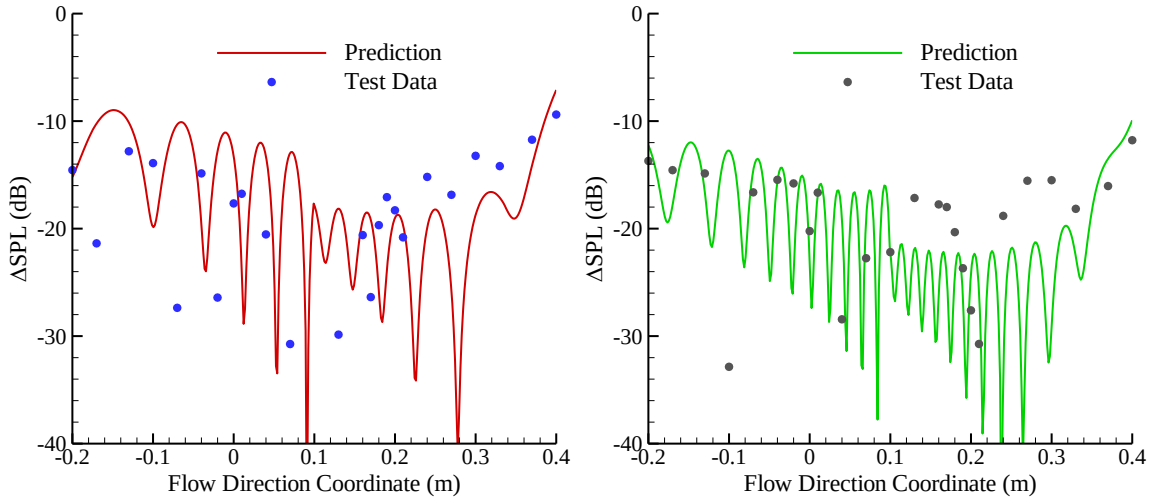

Fig. 25 Comparisons between test data and predictions for shifted flap at zero angle and 6.35 mm overhang for 10 kHz (left) and 20 kHz (right) for M=0 and the 70% source position.

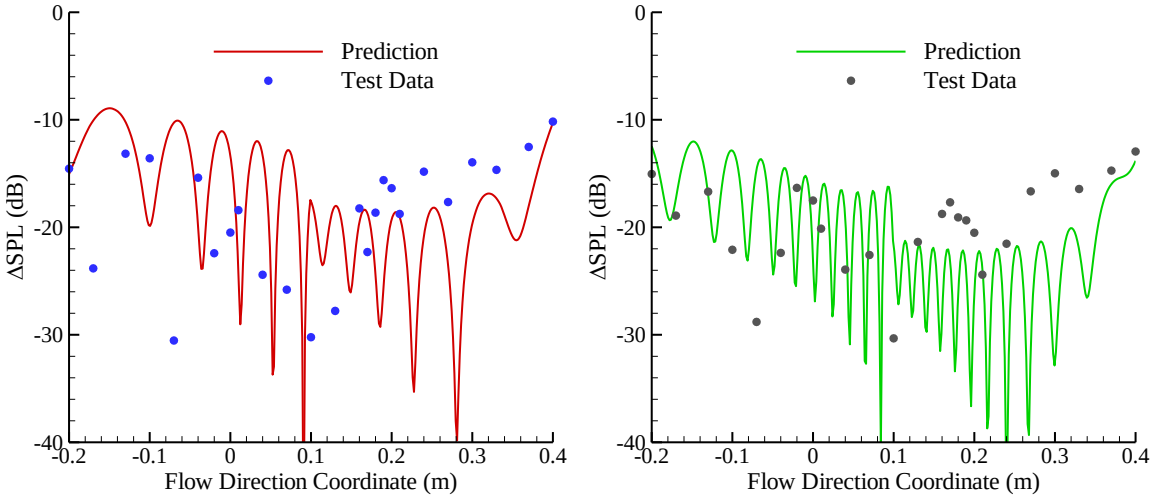

Fig. 26 Comparisons between test data and predictions for shifted flap at -10 degrees angle and 6.35 mm overhang for 10 kHz (left) and 20 kHz (right) for M=0 and the 70% source position.

The results presented in this section are only a subset of the test database, which includes many variations in source location, mean flow Mach number, and frequency. They are representative of other cases in the overall trends of the agreements and discrepancies between test data and predictions. The agreements show the correct modeling of major aspects in the computations. The discrepancies have various reasons, some of which are due to the metric and presentation of the results, some of which result from inevitable mismatch of test and computation, and some of which point to potential improvements needed from the prediction methodology.

One feature related to data presentation, discussed earlier in the section, is the measurement locations that are sparse and not sufficient to capture the interference patterns resulting from the highly coherent source and multiple propagation paths in the scattering. In most cases, the data measurement locations do not coincide with the peaks and dips of the interference patterns. This can lead to misleading and incorrect data trends and patterns if interpolation is used to connect the data points, either visually or computationally. Without the true trends from the data, the best approach for comparison is to examine the agreements at individual points. In all the figures presented in this section,

if the data points are simply connected, the resulting curves would look very different from the prediction curves, even though many data points are right on or close to the prediction curve.

Another feature that is also related to data presentation is the metric used in the comparisons. As stated previously, this section compared sound pressure level for exact frequencies in the computations and for frequency bands of 61 Hz in the data. For rapidly varying scattering patterns, there may be noticeable difference between the two frequency treatments. Even if the computations are done also for frequency bands, which is not a difficult effort, the comparisons with data may still be subject to irregular discrepancies because there are inevitably mismatches in some parameters between tests and computations. These mismatches may shift the interference patterns to amplify the discrepancies. Mismatches in test conditions can occur in many parameters, including source location, source dimension, measurement location, scattering geometry, and flow condition. For computations, these parameters are precisely defined to be mathematically exact. In tests, great care is always taken to ensure accurate values of these parameters. This is usually sufficient, but for highly oscillating scattering patterns, there may be noticeable errors. To avoid this, it is desirable to define quantities by integration and/or normalization, or other approaches to minimize the sensitivity of the results.

It should be noted that there are features in the tests that are not modeled or modeled differently in the computations. One example is the source dimensions. The laser spark source used in the test has been shown to be a good approximation of a theoretical monopole source, which leads to the model of point sources in the computations. However, the laser spark source is not a point source and has dimensions in the range of 2 to 5 mm. It is not clear at this time how the laser spark source of finite dimensions can be modeled in the computation methodology used in the present work, and if there is any noticeable impact to the scattering process. Another example is the scattering geometry. In the computations, the scattering bodies are modeled as smooth and rigid, but in the tests, the airfoil surfaces are treated with tripping devices to avoid flow separation. The roughness due to the tripping devices is tiny so that no significant effects are expected for mechanisms such as reflection because the acoustic wavelength is much larger than the dimensions of the roughness. It is, however, an open question whether and how the roughness can affect the smooth geometry diffraction from the airfoil leading edge, where the surface creeping waves propagating along the surface are the physical mechanism of the diffraction.

Some of the discrepancies in the comparison results are due to inadequate modeling in some aspects of the prediction methodology. One example is the low frequency correction. The methodology for the predictions is based on geometric acoustics, as discussed in Section III, and is theoretically applicable to high frequencies, or small wavelengths compared with typical dimensions in the scattering process. For the Shielding Flap geometry, the flap chord is 25.4 mm and the gap between the flap and the airfoil is 12.7 mm, which are both smaller than the wavelength of 34.5 mm at the frequency of 10 kHz. This in theory makes the geometric acoustics not applicable. To relax this restriction, a heuristic correction is implemented in the computations shown in this work. The correction has not been validated. One of the important objectives of the QFF tests is to provide data for validating the correction model and for identifying potential improvements. The comparisons, those presented in this section and those for other configurations, and the discrepancies revealed by the comparisons are valuable in achieving this objective.

V. Conclusions

A new noise reduction concept termed the Shielding Flap for a hybrid wing body aircraft configuration has been conceptually designed, and the acoustic propagation effects of relevant design parameters have been explored using a recent NASA-developed acoustic scattering prediction code. A large matrix of parameters was considered for a surrogate simplified configuration utilizing a two-dimensional airfoil. This yielded insights into the detailed scattering characteristics and acoustic impacts of varying parameters such as flap position and angle. These insights were used to downselect to a subset of parameters that were computed for a two-dimensional center-section of the MULDICON vehicle, which included the more complex scattering features of the target geometry. A three-dimensional calculation has not been completed but is necessary for a full understanding of the performance of a Shielding Flap. However, the computational results demonstrate that the Shielding Flap shows promise as an effective means to reduce three major sources of noise on the MULDICON vehicle, specifically turbomachinery noise, jet-trailing edge interaction noise, and jet noise. The optimal configuration of a Shielding Flap places the leading edge below and just forward of the jet nozzle trailing edge at a zero or positive angle of attack. This location maximizes shielding of the primary sources under consideration as well as the secondary diffracted source at the nozzle trailing edge, while simultaneously meeting practical requirements such as keeping the Shielding Flap far from the jet plume to avoid additional scrubbing or interaction noise sources.

More broadly, this work has demonstrated that the PAASc software can serve as an effective analysis tool for initial estimates of acoustic performance for a large test matrix of design parameters. Thousands of independent noise

scattering predictions were performed to build a database of results, from which the optimal configurations were selected. This is enabled by the geometric acoustics formulation upon which PAASc is built and expanded for use with aircraft noise scattering. The formulation allows for fast turnaround computation of either coherent or incoherent noise reflection, shielding, and diffraction with sharp and curved edges. Although several scattering cases involved small features outside of the applicable range of geometric acoustics, a heuristic correction to the method enabled at least a qualitative estimate of the scattering in these cases. While comparison between predicted and experimental results was complicated by several factors, including finite source dimensions, low measurement spatial resolution, and tripping devices on the experimental airfoil, overall trends observed in the experimental data confirmed the practical findings of the computational study.

Acknowledgments

The support of the NASA Advanced Air Transport Technology Project is gratefully acknowledged. The authors also wish to thank the NATO Science and Technology Organization for facilitating the collaborative effort organized under the NATO AVT-318 Task Group. Finally, the authors wish to thank the partner members of the NATO AVT-318 Task Group for many valuable discussions.

References

[1] June, J. C., Thomas, R. H., Guo, Y., and Clark, I. A., "Far Term Noise Reduction Technology Roadmap for a Large Twin-Aisle Tube-and-Wing Subsonic Transport," *25th AIAA/CEAS Aeroacoustics Conference*, Delft, The Netherlands, May 2019, AIAA Paper 2019-2428.

[2] Cummings, R. M., Liersch, C. M., and Schütte, A., "Multi-Disciplinary Design and Performance Assessment of Effective, Agile NATO Air Vehicles," *2018 Applied Aerodynamics Conference*, Atlanta, Georgia, June 2018, AIAA Paper 2018-2838.

[3] Hutcheson, F. V., Bahr, C. J., Thomas, R. H., and Stead, D. J., "Experimental Study of Noise Shielding by a NACA 0012 Airfoil," *2018 AIAA/CEAS Aeroacoustics Conference*, Atlanta, Georgia, June 2018, AIAA Paper 2018-2821.

[4] Thomas, R. H., Czech, M. J., and Doty, M. J., "High Bypass Ratio Jet Noise Reduction and Installation Effects Including Shielding Effectiveness," *51st AIAA Aerospace Sciences Meeting including the New Horizons Forum and Aerospace Exposition*, Grapevine, Texas, January 2013, AIAA Paper 2013-0541.

[5] Thomas, R. H., Burley, C. L., and Olson, E. D., "Hybrid Wing Body Aircraft System Noise Assessment with Propulsion Airframe Aeroacoustic Experiments," *International Journal of Aeroacoustics*, Vol. 11 (3+4), pp. 369-409, 2012.

[6] Clark, I. A., Thomas, R. H., and Guo, Y., "Aircraft System Noise of the NASA D8 Subsonic Transport Concept," *AIAA Journal of Aircraft*, Vol. 58, No. 5, pp. 1106-1120, 2021.

[7] Thomas, R. H., Burley, C. L., and Guo, Y., "Progress of Aircraft System Noise Assessment with Uncertainty Quantification for the Environmentally Responsible Aviation Project," *22nd AIAA/CEAS Aeroacoustics Conference*, Lyon, France, May 2016, AIAA Paper 2016-3040.

[8] June, J. C., Thomas, R. H., and Guo, Y., "System Noise Prediction Uncertainty Quantification for a Hybrid Wing-Body Transport Concept," *AIAA Journal*, Vol. 58, No. 3, pp. 1157-1170, 2020.

[9] Czech, M. J., Thomas, R. H., and Elkoby, R., "Propulsion Airframe Aeroacoustic Integration Effects for a Hybrid Wing Body Aircraft Configuration," *International Journal of Aeroacoustics*, Vol. 11, No. 3+4, pp. 335-367, 2012.

[10] Thomas, R. H., Burley, C. L., and Nickol, C. L., "Assessment of the Noise Reduction Potential of Advanced Subsonic Transport Concepts for NASA's Environmentally Responsible Aviation Project," *54th AIAA Aerospace Sciences Meeting*, San Diego, California, January 2016, AIAA Paper 2016-0863.

[11] Thomas, R. H. and Guo, Y., "Ground Noise Contour Prediction for a NASA Hybrid Wing Body Subsonic Transport Aircraft," *23rd AIAA/CEAS Aeroacoustics Conference*, Denver, Colorado, June 2017, AIAA Paper 2017-3194.

[12] Thomas, R. H., Guo, Y., Berton, J., and Fernandez, H., "Aircraft Noise Reduction Technology Roadmap Toward Achieving the NASA 2035 Goal," *23rd AIAA/CEAS Aeroacoustics Conference*, Denver, Colorado, June 2017, AIAA Paper 2017-3193.

[13] Guo, Y. Thomas, R. H., Clark, I. A., and June, J. C., "Far-Term Noise Reduction Roadmap for the Midfuselage Nacelle Subsonic Transport," *AIAA Journal of Aircraft*, Vol. 56, No. 5, pp. 1893-1906, 2019.

[14] Thomas, R. H., Guo, Y., Clark, I. A., and June, J. C., "Challenges and Opportunities for Subsonic Transport X-Plane Acoustic Flight Research," *2018 AIAA/CEAS Aeroacoustics Conference*, Atlanta, Georgia, June 2018, AIAA Paper 2018-3127.

[15] Zorumski, W. E., "Aircraft Noise Prediction Program Theoretical Manual," NASA TM-83199, 1982.
[16] Guo, Y. and Thomas, R. H., "Geometric Acoustics for Aircraft Noise Scattering," *28th AIAA/CEAS Aeroacoustics Conference*, Southampton, UK, June 2022, AIAA Paper 2022-3077.
[17] Thomas, R. H. and Guo, Y., "Systematic Validation of the PAAShA Shielding Prediction Method," *International Journal of Aeroacoustics*, Vol. 21, No. 5-7, pp. 558-584, 2022.
[18] Ahtye, W. F. and McCulley, G., "Evaluation of Approximate Methods for the Prediction of Noise Shielding by Airframe Components," NASA Technical Paper 1004, 1980.
[19] Hutcheson, F. V., Brooks, T. F., Burley, C. L., Bahr, C. J., Stead, D. J., and Pope, D. S., "Shielding of Turbomachinery Broadband Noise from a Hybrid Wing Body Aircraft Configuration," *20th AIAA/CEAS Aeroacoustics Conference*, Atlanta, Georgia, June 2014, AIAA Paper 2014-2624.
[20] Thomas, R. H., Guo, Y., Clark, I. A., and June, J. C., "Propulsion Airframe Aeroacoustics and Aircraft System Noise Flight Research Test: NASA Overview," *28th AIAA/CEAS Aeroacoustics Conference*, Southampton, UK, June 2022, AIAA Paper 2022-2993.
[21] Keller, J. B., "Geometrical Theory of Diffraction," *Journal of the Optical Society of America*, Vol. 52, No. 2, pp 116–130, 1962.
[22] Keller, J. B., "Rays, Waves and Asymptotics," *Bulletin of the American Mathematical Society,* Vol. 84, No. 5, pp 727-750, 1978.
[23] Lewis, R. M. and Boersma, J., "Uniform Asymptotic Theory of Edge Diffraction," *Journal of Mathematical Physics*, Vol. 10, No. 12, pp 2291–2305, 1969.
[24] Pierce, A. D., *Acoustics: An Introduction to its Physical Principles and Application*, McGraw-Hill, 1981.
[25] Dowling, A. P. and Ffowcs Williams, J. E., *Sound and Sources of Sound*, Ellis Horwood Publishers, 1983.
[26] Crighton, D. G., Dowling, A. P., Ffowcs Williams, J. E., Heckl, M., and Leppington, F. G., *Modern Methods in Analytical Acoustics*, Springer-Verlag, 1992.
[27] Morse, P. M. and Ingard, K. U., *Theoretical Acoustics*, McGraw-Hill, 1968.
[28] Sommerfeld, A., "Lectures on Theoretical Physics," *Optics*, Vol. IV, Academic Press, 1954.
[29] Levy, B. and Keller, J. B., "Diffraction by a Smooth Object," *Communications on Pure and Applied Mathematics*, Vol. 12, pp. 159–209, 1959.
[30] Agarwal, A., Dowling, A. P., Shin, H. C., Graham, W., and Sefi, S., "A Ray Tracing Approach to Calculate Acoustic Shielding by the Silent Aircraft Airframe," *12th AIAA/CEAS Aeroacoustics Conference (27th AIAA Aeroacoustics Conference)*, Cambridge, Massachusetts, May 2006, AIAA Paper 2006-2618.
[31] Agarwal, A. and Dowling, A. P., "The Calculation of Acoustic Shielding of Engine Noise by the Silent Aircraft Airframe," *11th AIAA/CEAS Aeroacoustics Conference (26th AIAA Aeroacoustics Conference)*, Monterey, California, May 2005, AIAA Paper 2005-2996.
[32] van Rens, J. R. P., van Rens, B. J. E., van Holten, T., and Ruijgrok, G. J. J., "Sound Level Prediction Using a Ray Tracing Algorithm for a Blended-Wing-Body," *6th AIAA/CEAS Aeroacoustics Conference*, Lahaina, Hawaii, June 2000, AIAA Paper 2000-2069.
[33] Lummer, M., "Maggi-Rubinowicz Diffraction Correction for Ray-Tracing Calculations of Engine Noise Shielding," *14th AIAA/CEAS Aeroacoustics Conference (29th AIAA Aeroacoustics Conference)*, Vancouver, British Columbia, Canada, May 2008, AIAA 2008-3050.
[34] Colas, D. F. M., "A Diffraction Integral Based Turbomachinery Noise Shielding Method," Master's Thesis, Department of Aeronautics and Astronautics, Massachusetts Institute of Technology, 2011.
[35] Guo, Y., Pope, D. S., Burley, C. L., and Thomas, R. H., "Aircraft System Noise Shielding Prediction with a Kirchhoff Integral Method," *23rd AIAA/CEAS Aeroacoustics Conference*, Denver, Colorado, June 2017, AIAA 2017-3196.